Second-order sound field during megasonic cleaning of patterned silicon wafers: Application to ridges and trenches

P. A. Deymier[a)]
Department of Materials Science and Engineering, University of Arizona, Tucson, Arizona 85721

J. O. Vasseur
Laboratoire de Dynamique et Structure des Matériaux Moléculaires, UPRESA CNRS 8024, UFR de Physique, Université des Sciences et Technologies de Lille, 59655 Villeneuve d'Ascq Cédex, France

A. Khelif
Laboratoire de Physique du Solide, Facultés Universitaires Notre Dame de la Paix, 61 rue de Bruxelles, B 5000 Namur, Belgium

S. Raghavan
Department of Materials Science and Engineering, University of Arizona, Tucson, Arizona 85721

(Received 17 May 2001; accepted for publication 2 July 2001)

We report calculations of first-order pressure and second-order pressure gradient fields in the neighborhood of patterned silicon wafers. The patterned wafers consist of a single ridge and two parallel ridges separated by a trench on a planar substrate. The efficacy of megasonic waves for cleaning patterned wafers contaminated with micron to submicron silica particles is discussed by comparing a removal force arising from the second-order pressure gradient to a van der Waals adhesion force. The calculated second-order pressure gradient fields show that acoustic energy may be concentrated in small volumes in the vicinity of pattern features with dimensions significantly smaller than the wavelength of the incident acoustic wave. The angle the incident acoustic wave makes with the planar substrate has a strong impact on the second-order pressure gradient field. Grazing incident waves appear to provide a more efficient way of cleaning inside a trench. Excitation of a trench resonant vibrational mode enhances the magnitude of the first-order pressure, the second-order pressure gradient, and therefore the removal force. © *2001 American Institute of Physics.* [DOI: 10.1063/1.1398595]

I. INTRODUCTION

Planar and patterned silicon wafers are routinely cleaned using megasonic waves during the manufacturing of semiconductor devices. During this process, the wafers are immersed in a water-based chemically active solution subjected to high power beams of acoustic waves. The frequency of these acoustic waves is typically in the interval 600 kHz–1 MHz. The direction of propagation differs whether one cleans a single wafer or multiple wafers are processed simultaneously.

Despite the success of this technology, the actual cleaning mechanism is still subject to debate. Several processes are believed to be operative, namely acoustic streaming, acoustic pressure gradients, microcavitation, and pressure enhanced chemical reactivity. In a recent publication[1] we calculated the second-order streaming force in a fluid in the vicinity of the solid/fluid interface for a silicon wafer immersed in water. The components of the streaming force parallel and normal to the silicon/water interface were determined as functions of frequency and wave vector of the incident acoustic wave. We also calculated the normal component of the removal force acting on a spherical contaminant particle adhering to the silicon surface. We found that the removal force is too small to remove submicron particles. In contrast the streaming force parallel to the solid/fluid interface appears to concentrate enough energy in a thin boundary layer near the surface to remove particles by pushing or rolling.

In most megasonic cleaning processes, the wavelength of the sound waves exceeds the dimensions of contaminant particles by orders of magnitude. We have shown that very small solid objects such as contaminant particles hardly scatter megasonic waves[2] leading to negligible forces due to the pressure gradient. In that study we limited ourselves to solving the linear wave propagation equation. In the present article we investigate the effect of nonlinear contributions to the pressure gradient on megasonic cleaning. Here we focus on the planar solid/liquid interface with features such as a ridge or trench. The ability of megasonic waves to remove contaminants from patterned silicon wafers has not been established clearly, especially cleaning between ridges or inside vias trenches in integrated circuits. In order to quantify the cleaning efficiency of megasonic waves we compare removal forces calculated from the nonlinear (second-order) pressure gradients in the vicinity of the feature to adhesion forces.

This article is organized as follows. In Sec. II we briefly review the methodology employed to calculate the nonlinear (second-order) sound field and removal forces. Results for the two systems we have studied, namely the planar interface with a ridge or a trench, are reported in Sec. III. Finally,

a)Electronic mail: deymier@u.arizona.edu

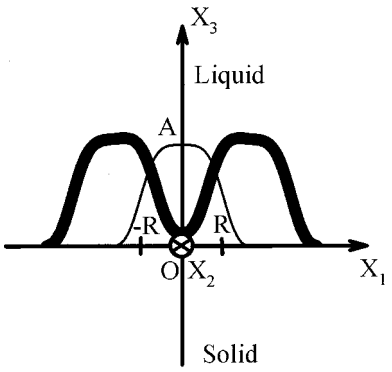

FIG. 1. Cross section of a single Gaussian ridge (thin line) and two Gaussian ridges separated by a trench (thick line). *A* and *R* measure the height and width of the raised features.

conclusions regarding megasonic cleaning of patterned wafers are drawn in Sec. IV.

II. MODELS AND METHODS

A. Models

In this article we consider two inhomogeneous systems composed of a rigid solid and a nonviscous fluid. These systems model patterned silicon wafers with an infinite ridge and an infinite trench, respectively. In the two cases the wafer fills the half space $X_3<0$ in the Cartesian coordinate system $(OX_1X_2X_3)$. The axis of the infinite raised feature or ridge is oriented parallel to the X_2 direction. We have assumed that its cross section has a Gaussian shape (see Fig. 1) defined in the (X_1OX_3) plane by

$$f(X_1)=A\exp\left[-\left(\frac{X_1}{R}\right)^4\right].$$

We have chosen the Gaussian shape for the sake of mathematical practicality.

We obtained a trench by constructing two Gaussian ridges. The cross section of the trench (double ridge) is given by

$$f(X_1)=A\exp\left[-\left(\frac{|X_1|}{R}-1.5\right)^4\right]+0.02\left(-2\frac{|X_1|}{R}+6\right),$$

$$-3\leqslant\frac{X_1}{R}\leqslant 3.$$

The linear term in the previous expression is added to the Gaussian function in order to slightly elevate the bottom of the trench with respect to the planar interface. This is necessary to avoid divergences in the computational method described below. In the preceding expressions, *A* controls the height of the ridge and *R* its width.

B. Calculation of the second-order acoustic field

1. General equations

The nonlinear motion in a viscous fluid, in the absence of external forces, is governed by the Navier–Stokes equation

$$\rho\left[\frac{\partial\mathbf{v}}{\partial t}+(\mathbf{v}\cdot\nabla)\mathbf{v}\right]=-\nabla p+\mu\nabla^2\mathbf{v}+\left(\mu'+\frac{1}{3}\mu\right)\nabla(\nabla\cdot\mathbf{v}), \tag{1}$$

where $\mathbf{v}$ is the velocity, ρ the density, μ and μ' the coefficients of shear and dilatation viscosity, and p the pressure. In this article, for the sake of simplicity, we treat the case of nonviscous fluids. In the limit of a fluid without viscosity, the Navier–Stokes equation reduces to the nonlinear Euler equation.

We briefly recall in this section the method used for determining the time-independent second-order solution to the nonlinear Euler equation. Following Nyborg's approach,[3] one makes the approximation that the fluid velocity, the excess pressure, and the excess density are written as the superposition:

$$\begin{aligned}&\mathbf{v}=\mathbf{v}^{(1)}+\mathbf{v}^{(2)},\\ &p-p^{(0)}=p^{(1)}+p^{(2)},\\ &\rho-\rho^{(0)}=\rho^{(1)}+\rho^{(2)}.\end{aligned} \tag{2}$$

Here, the terms $p^{(0)}$ and $\rho^{(0)}$ are the static pressure and the density of the fluid in the absence of acoustic field and are time and space independent. $\mathbf{v}^{(1)}$, $p^{(1)}$, and $\rho^{(1)}$ are first-order approximations to the nonlinear problem. These quantities vary sinusoidally in time with a pulsation ω. The second-order terms, $\mathbf{v}^{(2)}$, $p^{(2)}$, and $\rho^{(2)}$, are time-independent. Inserting Eq. (2) into the nonlinear Euler equation, eliminating all terms of order greater than two, averaging the remaining terms over several sonic cycles, and grouping the terms of the same order, yields the following equations

$$\nabla p^{(1)}=-\rho^{(0)}\frac{\partial\mathbf{v}^{(1)}}{\partial t}, \tag{3a}$$

$$\nabla p^{(2)}\equiv-\rho^{(0)}\langle(\mathbf{v}^{(1)}\cdot\nabla)\mathbf{v}^{(1)}+\mathbf{v}^{(1)}(\nabla\cdot\mathbf{v}^{(1)})\rangle. \tag{3b}$$

Equation (3a) gives the first-order pressure gradient versus the first-order velocity field and is formally equivalent to the equation of propagation of longitudinal waves in a nonviscous fluid. In the limit of a very low compressible fluid, such as water, the terms $\rho^{(1)}$ and $\rho^{(2)}$ in Eq. (2) are negligible compared to $\rho^{(0)}$ and $\rho\approx\rho^{(0)}$. Then Eq. (3a) may be rewritten as

$$\Delta p^{(1)}-\frac{1}{c_l^2}\frac{\partial^2 p^{(1)}}{\partial t^2}=0, \tag{4}$$

where c_l is the longitudinal speed of sound in the fluid. In Eq. (3b) the brackets, $\langle\,\rangle$, indicate that a time average is taken over several sonic cycles in order to retain only these terms that are time independent.

2. Ridge and trench

We initially calculate the first-order pressure gradient and then deduce the first-order velocity field. With Nyborg' approach, the first-order velocity field is then used to obtain a second-order approximation of the pressure gradient according to Eq. (3b). For the sake of simplicity we reduce the problem to two dimensions and consider only wave propa-

gation in the plane (X_1OX_3) perpendicular to the axis of the ridge or trench. The first-order pressure gradient, assumed to be a harmonic function of time, takes the form in complex notation

$$p^{(1)}(X_1,X_3,t)=p^{(1)}(X_1,X_3)e^{-i\omega t}, \tag{5}$$

and Eq. (4) may be rewritten as

$$\frac{1}{\rho^{(0)}}\left(\frac{\partial}{\partial X_1^2}+\frac{\partial}{\partial X_3^2}+\frac{\omega^2}{c_l^2}\right)p^{(1)}(X_1,X_3)=0. \tag{6}$$

We must solve Eq. (6) for the liquid motion subject to the boundary condition $\nabla p^{(1)}=0$ in the direction perpendicular to the solid–liquid interface. This boundary condition is equivalent to the condition of continuity of the acoustic displacement along the normal to the rigid solid/nonviscous fluid interface. For this we employ a method based on Green's functions which has already been exposed in Ref. 2. This method allows one to write the pressure field, $p^{(1)}\times(D)$, in the fluid bounded by a surface supporting a linear feature in the form

$$p^{(1)}(D)=p_{\mathrm{si}}^{(1)}(D)+g_b(D,M)T_b(M,M)p_{\mathrm{si}}^{(1)}(M). \tag{7}$$

Equation (7) is an integral equation where summations over the positions belonging to the space of the interface between the ridge or the trench and the fluid, M, is implicit. D represents the space encompassing the entire fluid. The terms g_b and $p_{\mathrm{si}}^{(1)}$ are the Green's function of the semi-infinite fluid bounded by a rigid planar surface at $X_3=0$ and the pressure field associated with g_b, respectively. $T_b(M,M)$ is a scattering function defined in the space M.

From a practical point of view we consider the case of an incident compression wave traveling towards the surface with an incident angle θ_i. Because the acoustic wave is reflected by the rigid planar surface, the pressure field in the semi-infinite liquid in complex notation, $\tilde{p}_{\mathrm{si}}^{(1)}(D)$, takes the following representation

$$\tilde{p}_{\mathrm{si}}^{(1)}(X_1,X_3)=\frac{W}{2}\left\{\exp\left[\frac{i\omega}{c_l}(X_1\sin\theta_i-X_3\cos\theta_i)\right]+\exp\left[\frac{i\omega}{c_l}(X_1\sin\theta_i+X_3\cos\theta_i)\right]\right\}, \tag{8}$$

where $W/2$ is the amplitude of the incident pressure wave. For $\theta_i=0$, Eq. (8) yields a standing wave varying like $\cos((\omega/c_l)X_3)$.

In order to obtain the scattering function and the pressure field, one solves numerically the integral equation (7). For this we discretize space which transforms these equations into discrete matrix relations. For this purpose, the axis X_l is divided into $2N$ intervals. In this way, the continuous curve delimiting the interfacial space M is divided into small segments. In practice N is chosen to be large enough to have a good balance between convergence and computation time. Further details of the calculation as well as the numerical procedure are given in Refs. 4 and 5.

Since the fluid undergoes harmonic motion with a time dependence according to $e^{-i\omega t}$, the first-order velocity field is obtained from Eq. (3a), as $\tilde{\mathbf{v}}^{(1)}=(-i/\omega\rho^{(0)})\nabla p^{(1)}$. With this, Eq. (3b) may be written in complex notation as

$$\nabla p^{(2)}=-\rho^{(0)}\frac{1}{2}\mathrm{Re}\begin{pmatrix} 2\tilde{\nu}_1^{(1)}\dfrac{\partial\tilde{\nu}_1^{(1)*}}{\partial X_1}+\left(\tilde{\nu}_3^{(1)}\dfrac{\partial\tilde{\nu}_1^{(1)*}}{\partial X_3}+\tilde{\nu}_1^{(1)}\dfrac{\partial\tilde{\nu}_3^{(1)*}}{\partial X_3}\right) \\ 0 \\ 2\tilde{\nu}_3^{(1)}\dfrac{\partial\tilde{\nu}_3^{(1)*}}{\partial X_3}+\left(\tilde{\nu}_3^{(1)}\dfrac{\partial\tilde{\nu}_1^{(1)*}}{\partial X_1}+\tilde{\nu}_1^{(1)}\dfrac{\partial\tilde{\nu}_3^{(1)*}}{\partial X_1}\right)\end{pmatrix}, \tag{9}$$

where the asterisk stands for the complex conjugate quantity. All derivatives in the computational method are calculated with a symmetric finite difference method.

C. Removal and adhesion forces

We consider the effect of the second-order sound field on cleaning efficiency. In Ref. 1 we have shown that in first approximation, a contaminant particle of volume V in the fluid is subjected to a force

$$\mathbf{f}=\int_V \nabla p_2 dV. \tag{10}$$

Here we have made the assumption that the contaminant particle does not perturb the first-order sound field. In the case of small particles compared to the scale of the variations in the second-order pressure gradient, Eq. (10) may be simplified as the product of the gradient and the volume of the particle. The removal force is consequently colinear and points in the same direction as the second-order pressure gradient. A contaminant particle adhering to the surface of a wafer may be removed, during megasonic cleaning, if the force given by Eq. (10) counteracts the London–van der Waals adhesion force, usually considered to be the dominant attractive force for short distances in particle adhesion.[6] The van der Waals force of adhesion between a spherical particle of radius r_0 and a surface is given by[7]

$$f_{\mathrm{vdW}}=\frac{A_{132}r_0}{6(d-r_0)^2}, \tag{11}$$

where d is the distance of the center of the particle to the surface. The effective Hamaker constant, A_{132}, is a function of the material constituting the particle (material 1), the sur-

face (material 2), and the medium surrounding the particle/surface system (material 3). Here we consider the case of a silica contaminant particle in water adhering to a wafer coated with a thin layer of silica. The Hamaker constant for that system is $A_{132}=0.83\times10^{-20}$ J.[8,9] In the case of a particle nearly in contact with the surface, the separation distance $d-r_0$ is only on the order of a few angstroms.[10]

III. RESULTS

All results presented below are for ridges and trenches with $A=2R$, that is an aspect ratio of 1:1. For reasons of convergence of the numerical algorithms we have limited our calculations to reduced frequencies in the range $0.1\leqslant\omega^*\leqslant0.5$, where $\omega^*=\omega R/c_l$. The first-order pressure is reported in units of *W*. To obtain more manageable values for the second-order pressure gradient we define a scaled pressure gradient, $\nabla\hat{p}^{(2)}$, by $\nabla p^{(2)}=\nabla\hat{p}^{(2)}(c_l^2W^2/R)10^{-20}$ N m^{-3}. The discretization of the interface domain for the ridge and the trench (dual ridges) is done with $N=300$ and $N=500$, respectively.

In Secs. III A and III B we report two-dimensional contour maps of the first-order pressure and the second-order pressure gradient around a single ridge and a trench. The implication of the sign (direction) of the gradient on particle removal is discussed in a qualitative manner in these same sections. A more quantitative discussion and comparison between the removal forces and the adhesion forces is given in Sec. III C.

A. Ridge

The effects of frequency on the first-order pressure field in the case of an incident plane wave perpendicular to the planar substrate ($\theta_i=0$) is reported in Figs. 2(a) and 2(b). These figures are two-dimensional contour maps of the pressure around the raised feature with lines representing isobars. For an angular frequency $\omega^*=0.1$, the wavelength of the standing wave amounts to $2\pi R/\omega^*=20\pi R$. This wavelength is significantly larger than the size of the ridge. The pressure field is distorted in the vicinity of the ridge in order to satisfy the continuity condition of the displacement at the solid/liquid interface. At higher frequency and shorter wavelength the ridge scatters the incident wave leading to more significant modifications of the isobars. Figures 3 and 4 illustrate the spatial variations of the second-order pressure gradient at the two frequencies 0.1 and 0.5. The magnitude and direction of the components of the gradient are given as contour maps of $\mathrm{sgn}(\nabla\hat{p}_i^{(2)})\log(|\nabla\hat{p}_i^{(2)}|)$ with $i=1,3$. A negative sign indicates that the gradient is oriented along the direction of the negative X_i's. The indicated value is a measure of the order of magnitude of the gradient. $\nabla\hat{p}_1^{(2)}$ is an antisymmetrical function of X_1 for both frequencies while $\nabla\hat{p}_3^{(2)}$ is symmetrical.

In relation to removing contaminant particles near ridges, since the removal force is parallel to the second-order pressure gradient, it is worth noting that in the direction X_1, the pressure gradient points away from the ridge, this is for both frequencies. At high frequencies $\nabla\hat{p}_3^{(2)}$ changes sign several times around the raised feature. In contrast lower

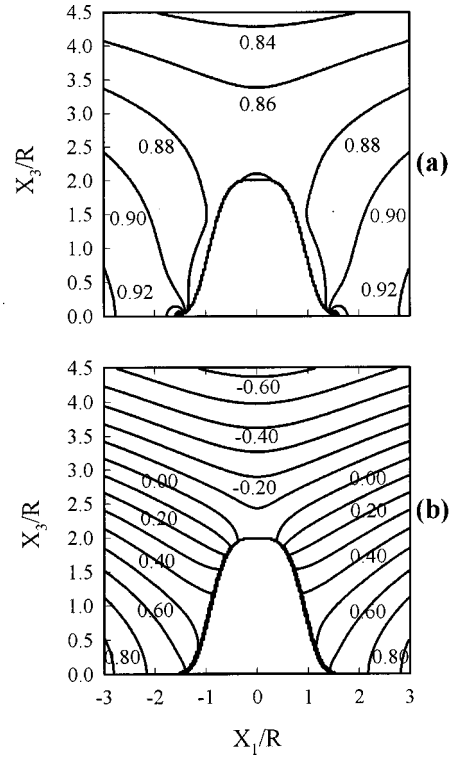

FIG. 2. First-order pressure fields around a ridge for a normal incident wave with (a) $\omega^*=0.1$ and (b) $\omega^*=0.5$. The pressure is in units of W (the amplitude of the incident wave) and spatial dimensions are in units of R.

frequencies appear to be more favorable to efficient cleaning as $\nabla\hat{p}_3^{(2)}$ remains essentially positive in a region surrounding the ridge with thickness on the order of *R*. The magnitudes of the components of the scaled pressure gradient are not greater than 10^4.

At the frequency $\omega^*=0.1$ we have also investigated the effect of the angle of incidence θ_i. We have considered the case of a grazing wave (nearly parallel to the X_1 axis), launched from the $X_1<0$. Here, in absence of the ridge, the first-order isobars would be perpendicular to the planar substrate. The ridge forces the isobars to become parallel to X_1 near its top. The most significant effect on both components of the second-order pressure gradient is to alternate its sign numerous times around the raised feature. The magnitude remains similar to that of a normal incident wave. In terms of the direction of the removal forces, a grazing wave appears to be less conducive to effective cleaning around the ridge.

B. Trench

As in the case of the ridge we initially investigate normal incident waves, with reduced frequency 0.1 and 0.5. In Figs. 5(a) and 5(b) we show the first-order isobars for these two frequencies. Again at $\omega^*=0.1$, the isobars are only affected in the near vicinity of the raised features as well as inside the trench. At $\omega^*=0.5$, the first-order pressure map is drastically perturbed and the corresponding isobars differ significantly from those calculated for a single ridge. The gradient amplitude decreases below -1 inside the trench. The isobars take the form of a nearly spherical pressure wave originating from the trench. This can be explained in terms of a resonating

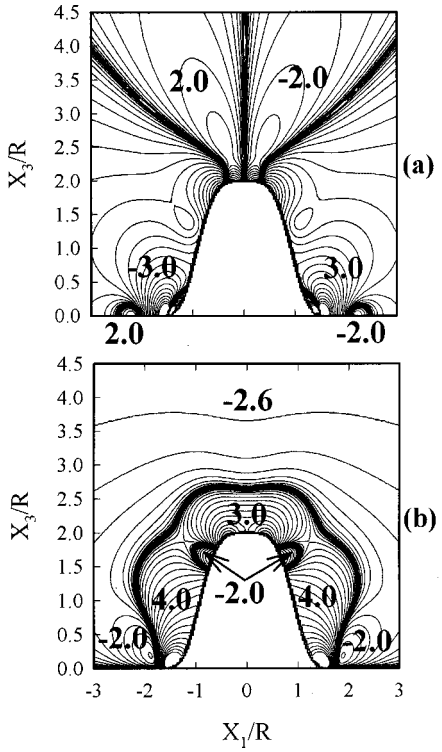

FIG. 3. Second-order pressure gradient field near a ridge for $\omega^*=0.1$ given as contour maps of $\mathrm{sgn}(\nabla\hat{p}_i^{(2)})\log(|\nabla\hat{p}_i^{(2)}|)$ for (a) $i=1$ and (b) $i=3$. The incident wave is normal to the substrate. Thick lines correspond to zero gradients. A number with negative sign means that the gradient is oriented along the direction of the negative X's. The number indicates the largest order of magnitude of the scaled gradient $\nabla\hat{p}_1^{(2)}$. The interval between two successive contour lines is equal to 0.2.

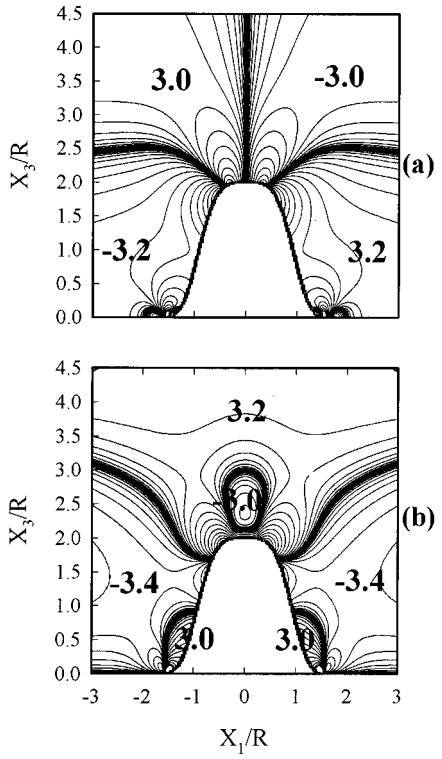

FIG. 4. Same as Fig. 3 but for $\omega^*=0.5$.

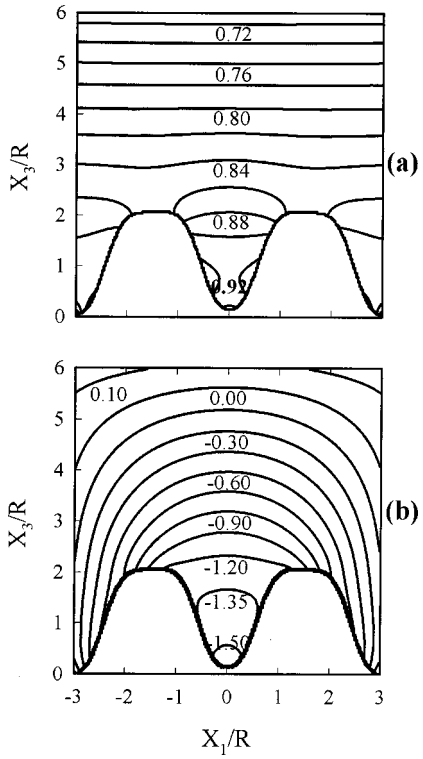

FIG. 5. Same as Fig. 2 but for two ridges separated by a trench.

trench. The problem of propagation of longitudinal waves in a nonviscous fluid bound by a rigid substrate with two rigid ridges is isomorphic to the problem of propagation of transverse waves in a semi-infinite elastic solid, bound by a vacuum, in which two trenches are cut. The elastic material separating the two trenches in that latter system is therefore equivalent to the trench filled with fluid that we study. This elastic material may be viewed as a single elastic ridge. It has been shown that an elastic ridge with an aspect ratio of 1:1 exhibits resonating vibrational modes near a reduced frequency of 0.5.[11] The trench filled with liquid will therefore resonate at the same reduced frequency, thus explaining the large amplitude of the first-order pressure inside the trench.

In Figs. 6(a) and 6(b) we present the components of the second-order pressure gradient in the neighborhood of the trench at the lowest frequency considered. As was the case for the single ridge, $\nabla\hat{p}_1^{(2)}$ is antisymmetric. The interior of the trench is separated by a line of zero gradient. The gradient $\nabla\hat{p}_1^{(2)}$ points away from the inside surfaces of the trench, thus favoring the removal of any contaminant particle that may adhere to the side walls of the trench. The maximum magnitude of $\nabla\hat{p}_1^{(2)}$ is of the order of 10^3 inside the trench. The component of the second-order pressure gradient along X_3, $\nabla\hat{p}_3^{(2)}$, shown in Fig. 6(b) changes sign several times as one moves up from the bottom of the trench. This gradient points upward in a region near the bottom of the trench and does not exceed a magnitude of 10^4. Removal of contaminant particles sitting at the bottom of the trench may therefore be possible. Most of the central region of the trench is subjected to a negative gradient opposing particle removal. Positive gradients occur again near the top portion of the trench. The second-order pressure gradient calculated with

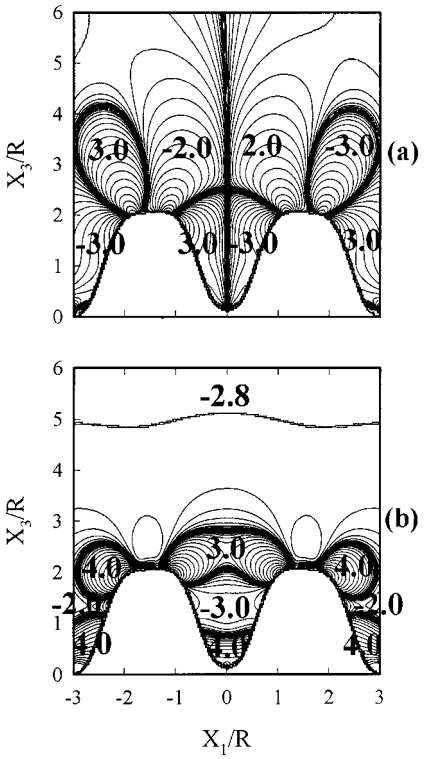

FIG. 6. Same as Fig. 3 but for the two-ridge (trench) system and $\omega^* = 0.1$.

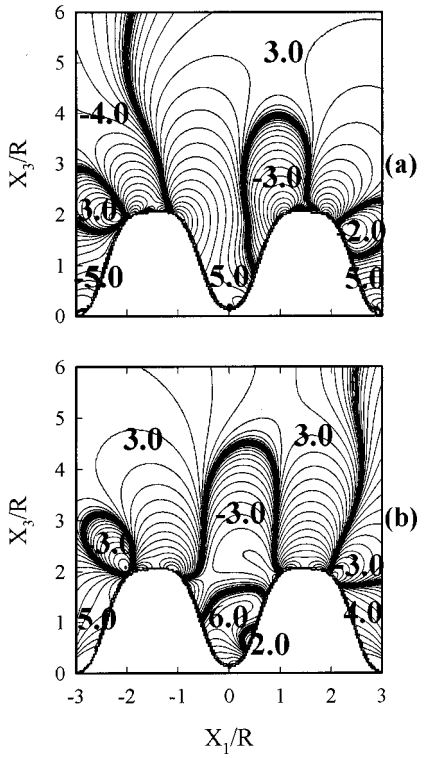

FIG. 8. Same as Fig. 6 but for a grazing wave.

the larger reduced frequency of 0.5 [see Figs. 7(a) and 7(b)], exhibits a similar behavior as its lower frequency counterpart. Most notable is the magnitude of $\nabla \hat{p}_3^{(2)}$ at the bottom of the trench that can be of the order of 10^6, at least two orders of magnitude more than in the absence of resonance.

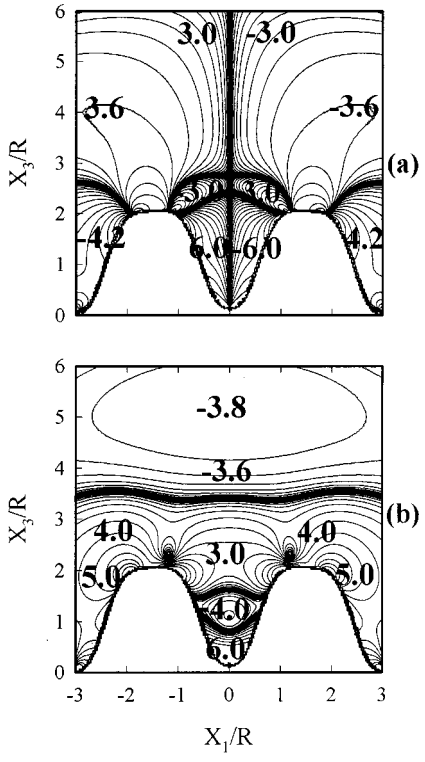

FIG. 7. Same as Fig. 6 but for $\omega^* = 0.5$.

Figures 8(a) and 8(b) show the effect of the angle of incidence on the distribution of the second-order pressure gradient. We consider the lowest frequency $\omega^* = 0.1$ and a grazing incident wave. In contrast with the normal wave, $\nabla \hat{p}_1^{(2)}$ is not antisymmetric. Compared to Fig. 6(a), the line of zero gradient that separated the trench in half (at $X_1 = 0$) has been shifted to $X_1 \approx 0.5R$. This component is now positive over most of the trench and takes on values of the order of 10^5 in that region. When comparing $\nabla \hat{p}_3^{(2)}$ for the grazing wave [Fig. 8(b)], with that corresponding to the normal wave [Fig. 6(b)], we observe that the region of positive values extends over most of the volume of the trench without significant change in its magnitude. The case of a grazing wave appears to provide a more extensive cleaning of the interior of the trench.

C. Discussion

In Sec. III A and III B we have discussed the impact of the sign of the second-order pressure gradient (and the removal force) on acoustic cleaning in the vicinity of a single ridge and inside a trench. Here we compare quantitatively the removal force that results from the second-order pressure gradient to the adhesion force of a spherical particle. The speed of sound in water and the density of this fluid are taken as $c_l = 1531\ \mathrm{m\,s^{-1}}$ and $\rho^{(0)} = 1000\ \mathrm{kg\,m^{-3}}$, respectively. In the usual megasonic cleaning processes transducer power may vary up to a few hundred watts. The area cross section of the transducer amounts to a few centimeters square, thus the acoustic intensity I_0 may range from a few $\mathrm{W\,cm^{-2}}$ to a few tens $\mathrm{W\,cm^{-2}}$. The pressure amplitude of the incident wave, W, is given in terms of the acoustic intensity by

TABLE I. Calculated van der Waals adhesion force and particle removal force as functions of particle radius.

		f_{removal} (N)			
$r_0(\mu\text{m})$	f_{vdW} (N)	Ridge: 1–5 MHz, 25 μm Nonresonating trench: 1 MHz, 25 μm	Ridge: 25–125 MHz, 1 μm Nonresonating trench: 25 MHz, 1μm	Resonating trench: 5 MHz, 25 μm	Resonating trench: 125 MHz, 1 μm
1	1.38×10^{-9}	8.81×10^{-11}		8.81×10^{-9}	
0.5	6.92×10^{-10}	1.10×10^{-11}		1.10×10^{-9}	
0.25	3.46×10^{-10}	1.38×10^{-12}	3.45×10^{-11}	1.38×10^{-10}	3.45×10^{-9}
0.1	1.38×10^{-10}	8.81×10^{-14}	2.20×10^{-12}	8.81×10^{-12}	2.20×10^{-10}

$W=\sqrt{2\rho^{(0)}c_l I_0}$.[12] Therefore we choose values of W ranging from 3 to 15 atm. Since the computational method that we used for resolving the acoustic problem was limited to reduced frequencies larger than $\omega^*=\omega R/c_l=0.1$, the radius of the raised features we considered in this work depends on the frequency of the acoustic wave. For instance, when using the frequency $\nu=1$ MHz (i.e., an angular frequency $\omega=6.28\times10^6\,\text{rad}\,\text{s}^{-1}$), the features must be larger than 25 μm. In order to investigate cleaning efficiency of micron size features we need to consider significantly higher frequencies ($\upsilon\approx25$ MHz) than that used routinely in most megasonic cleaning equipment. The subsequent discussion is therefore limited to four physical cases: (1) $\nu=1$ MHz and $R=25\,\mu$m, (2) $\nu=25$ MHz and $R=1\,\mu$m, (3) $\nu=5$ MHz and $R=25\,\mu$m, and (4) $\nu=125$ MHz and $R=1\,\mu$m. Contaminant particles with radii $r_0=1$, 0.5, 0.25, and 0.1 μm and a separation distance $(d-r_0)=10$ Å are chosen. We have seen in Secs. A and B that the magnitude of the components of the scaled second-order pressure gradient, $\nabla\hat{p}^{(2)}$, for a ridge ($\omega^*=0.1$,0.5) or a trench in absence of vibrational resonance ($\omega^*=0.1$) does not exceed 10^4. A resonating trench ($\omega^*=0.5$) may increase that magnitude at its bottom up to 10^6. We use these most favorable magnitudes as well as the highest pressure amplitude $W=15$ atm to calculate upper limits of the removal forces. Table I summarizes the results for the four physical cases relevant to the ridge and to the trench as well as the adhesion forces acting on a contaminant particle with the four different radii. For a ridge and a trench with $R=1\,\mu$m, removal forces can only be estimated for the two smallest particle radii. For particle radii on the order of the ridge or trench size, one would expect significant modifications of the first-order pressure field and by consequence of the second-order pressure gradient. The optimum removal force exceeds the adhesion force only for frequencies near the resonant frequency of the trench. For all other geometry and frequency, the removal force dominates and the second-order acoustic field is unable to lift contaminant particles. However, it is necessary to recall that the adhesion force that we are using in Table I is that of a particle interacting with a semi-infinite medium with a flat surface and that this force is normal to the surface. This choice of adhesion force is proper for a contaminant particle sitting at the bottom of a trench. Particles adhering to the side of a ridge or the sidewall of a trench may be subjected to removal forces that are parallel to the sidewall. These forces and their associated moment may provide a cleaning mechanism by which the particles are rolled along the wall surface. We would like to also note that the calculation of the second-order pressure gradient presented in this article is for a nonviscous fluid. That is, the acoustic field must satisfy a condition of continuity of the displacement perpendicular to the solid/fluid interface only. In the case of a viscous fluid the acoustic displacement must also satisfy a condition of continuity in the directions parallel to the solid/fluid interface. This condition will give rise to sharp variations in the displacement and velocity field within the so-called acoustic boundary layer. The thickness of that boundary layer scales as $\sqrt{\mu/\omega\rho_0}$ with μ the viscosity of the fluid. For water, at megasonic frequencies, the acoustic boundary layer thickness is on the order of 1 μm. The additional condition for continuity should therefore enhance the magnitude of the second-order pressure gradient [1] in the near vicinity of the ridge or the trench leading to larger removal forces than those calculated in the present study. It is therefore not improbable for the removal force around a ridge or inside a trench to exceed the adhesion force even at frequencies that do not stimulate resonating modes of vibration.

IV. CONCLUSIONS

We have undertaken an investigation of the second-order (time independent) pressure gradient field in the vicinity of patterned silicon wafers immersed in a fluid. We have considered two geometries, namely a single ridge and two ridges forming a trench on a planar substrate. The first-order acoustic field is calculated using methods based on Green's functions. The second-order pressure gradient is obtained within the context of Nyborg's perturbation theory. The time-independent pressure gradient is related to a removal force acting on a contaminant particle and compared to the van der Waals adhesion force between the particle and a planar substrate. The methodology we employed has some severe limitations. First, the fluid is nonviscous but corrections to the second-order pressure gradient due to viscosity are expected to enhance the magnitude of the gradient and therefore cleaning efficiency.[1] Second, the reduced frequency, $\omega^*=\omega R/c_l$ must be larger than 0.1 as uncontrollable numerical uncertainties arise for lower values. This latter condition imposes a lower limit on the trench and ridge dimensions that can be investigated (i.e., >1 μm) at megasonic frequencies. These dimensions are in excess of feature linewidths (<1 μm) in

current integrated circuits. In spite of these limitations several important conclusions concerning megasonic cleaning of patterned wafers can be drawn.

(1) The second-order pressure gradient may take on non-negligible values around ridges or inside trenches, i.e., acoustic energy may be concentrated in small volumes in the vicinity of pattern features with dimensions significantly smaller than the wavelength of the incident acoustic wave.

(2) The angle the incident acoustic wave makes with the planar substrate appears to play a very important role in the sign of the second-order pressure gradient near a ridge or inside a trench. In particular more efficient cleaning inside a trench may be achieved by varying the angle from an incoming wave with a normal incidence to a grazing wave.

(3) Cleaning efficiency inside a trench may be improved by employing higher frequencies than are currently used. More specifically, excitation of a trench resonant vibrational mode enhances the magnitude of the second-order pressure gradient (and therefore the removal force). It is noteworthy that the resonant reduced frequency of an elastic ridge (and therefore of a trench filled with fluid) decreases with increasing aspect ratio.[11] This may allow megasonic cleaning of deep but narrow trenches.

(4) The magnitude of the second-order pressure gradient (and removal force) increases linearly with the output power density of the incident megasonic wave.

ACKNOWLEDGMENTS

This research was supported by a grant from the Center for Micro-contamination Control at the University of Arizona. J.O.V. and A.K. would like to acknowledge the Department of Materials Science and Engineering at the University of Arizona for its hospitality.

[1] P. A. Deymier, J. O. Vasseur, A. Khelif, B. Djafari-Rouhani, L. Dobrzynski, and S. Raghavan, J. Appl. Phys. **88**, 6821 (2000).
[2] P. A. Deymier, A. Khelif, J. O. Vasseur, B. Djafari-Rouhani, and S. Raghavan, J. Appl. Phys. **88**, 2423 (2000).
[3] W. L. Nyborg, *Acoustic Streaming, Physical Acoustics*, edited by W. P. Mason (Academic, London, 1965), Vol. IIB, Chap. 11.
[4] B. Djafari-Rouhani and L. Dobrzynski, J. Phys.: Condens. Matter **5**, 8177 (1993).
[5] A. Khelif and B. Djafari-Rouhani, J. Appl. Phys. **81**, 7141 (1997).
[6] D. Zhang, Ph.D. dissertation, University of Minnesota, 1993.
[7] M. B. Renade, Aerosol. Sci. Technol. **7**, 161 (1987).
[8] J. Visser, Adv. Colloid Interface Sci. **3**, 331 (1972).
[9] J. Israelachvilii, *Intermolecular & Surface Forces*, 2nd ed. (Academic, San Diego, 1994).
[10] W. C. Hinds, *Aerosol Technology* (Wiley, New York, 1982).
[11] B. Djafari-Rouhani, L. Dobrzynski, and A. Khelif, Prog. Surf. Sci. **48**, 301 (1995).
[12] G. Gale, A. Busnania, F. Dai, and I. Kashkouch, Semicond. Int. **19**, 133 (1996).